Ultrafast quasiparticle relaxation dynamics in normal metals and heavy-fermion materials

K. H. Ahn, M. J. Graf, S. A. Trugman, J. Demsar,* R. D. Averitt, J. L. Sarrao, and A. J. Taylor
Los Alamos National Laboratory, Los Alamos, New Mexico 87545, USA

(Received 11 August 2003; published 30 January 2004)

We present a detailed theoretical study of the ultrafast quasiparticle relaxation dynamics observed in normal metals and heavy-fermion materials with femtosecond time-resolved optical pump-probe spectroscopy. For normal metals, a nonthermal electron distribution gives rise to a temperature- (T) independent electron-phonon relaxation time at low temperatures, in contrast to the T^{-3}-divergent behavior predicted by the two-temperature model. For heavy-fermion compounds, we find that the blocking of electron-phonon scattering for heavy electrons within the density-of-states peak near the Fermi energy is crucial to explain the rapid increase of the electron-phonon relaxation time below the Kondo temperature. We propose the hypothesis that the slower Fermi velocity compared to the sound velocity provides a natural blocking mechanism due to energy and momentum-conservation laws.

DOI: 10.1103/PhysRevB.69.045114 PACS number(s): 71.27.+a, 78.47.+p, 71.10.−w

I. INTRODUCTION

Recently, ultrafast time-resolved optical spectroscopy has been used to reveal the nature of the quasiparticle relaxation dynamics in condensed-matter systems. Femtosecond time-resolved pump-probe optical measurements have been carried out in normal metals,[1,2] conventional[3] and high-T_c superconductors,[4] and charge-density wave solids.[5] Time-resolved terahertz spectroscopy has measured picosecond time-scale transient conductivity in colossal magnetoresistance manganites.[6] These experiments show directly in the time domain how constituent degrees of freedom of materials interact with each other, which is important to understand the physics governing the ground state and the low-energy excited states of materials. Understanding the fast dynamics of quasiparticles is also crucial for technological applications of these materials, for example, in the design of very fast switching devices.

We recently reported femtosecond time-resolved pump-probe optical measurements on $LuAgCu_4$ and $YbAgCu_4$.[7] These two materials are isostructural with a negligible difference in lattice constants[8] (about 0.3%) and about 1% difference in atomic mass between Lu and Yb. However, their electronic structures are strikingly different due to the *f*-level occupancies in Lu and Yb. The closed-shell $4f$ levels in Lu have no significant interaction with Cu $3d$ and Ag $4d$ conduction electrons, and $LuAgCu_4$ is a normal metal.[9] In contrast, the open-shell $4f$ levels in Yb, that is, the localized hole in the $4f^{13}$ configuration, have a strong interaction with conduction electrons, and make $YbAgCu_4$ a heavy-fermion material, which is characterized by a large peak in the electron density of states (DOS) at the Fermi energy (E_F) and, equivalently, a large Sommerfeld coefficient γ.[10,11] Our time-resolved optical experiments show very different relaxation dynamics in these two materials. $LuAgCu_4$ shows a relaxation time (τ) versus temperature (T) behavior similar to other normal metals, such as Ag and Au.[1,2] In particular, there is very little T dependence in τ at low temperatures. However, $YbAgCu_4$ shows approximately a 100-fold increase in τ, as T is decreased from the Kondo temperature (T_K) down to 10 K. The Kondo temperature is about 100 K in $YbAgCu_4$ and typically characterizes the width of the large DOS near E_F.

In Ref. 7, we presented experimental data showing different relaxation dynamics in $LuAgCu_4$ and $YbAgCu_4$ along with the main theoretical ideas and final results of the calculations based on coupled electron and phonon Boltzmann transport equations. In this paper, we report on the details of the theoretical model and analysis, and clarify the underlying physics. The theories that existed before our study are summarized in Sec. II A. Sections II B and III discuss our calculations of the relaxation dynamics in normal metals and heavy-fermion materials, respectively. Section IV summarizes our results.

II. NORMAL METALS

A. Two-temperature model, its inconsistency with experiments, and the nonthermal electron model

In ultrafast optical pump-probe spectroscopy, an ultrafast laser pulse initially excites the electron system, and the probe pulse monitors the relaxation of the electron system by measuring transient optical properties with subpicosecond time resolution. Because the diffusion of heat out of the illuminated (probed) region is much slower (tens to hundreds of nanoseconds) than the time scales of interest, the relaxation of the excited electrons is due to the thermalization among electrons and other degrees of freedom, such as phonons, within the illuminated areas.

The most commonly used model for the relaxation dynamics of photoexcited electrons in metals is called the two-temperature model (TTM),[12] which assumes much faster relaxation *within* each constituent system (e.g., electron system, phonon system) compared to the relaxation *between* these constituent systems. In this approximation, the temperature of each system can be defined during relaxation, and the relaxation time τ between systems 1 and 2 is determined by their specific heats C_1 and C_2 and the energy-transfer rate per temperature difference, $g(T)$:[13]

$$\frac{1}{\tau}=g(T)\left(\frac{1}{C_1}+\frac{1}{C_2}\right). \tag{1}$$

Kaganov, Lifshitz, and Tanatarov[12] calculated the energy-transfer rate $g(T)$ between electrons (e) and phonons (p) in normal metals by solving coupled Boltzmann transport equations for electrons and phonons with thermal equilibrium distributions at different temperatures. Their results predict $\tau \sim T$ at $T>T_{Debye}/5$ and $\tau \sim T^{-3}$ at $T<T_{Debye}/5$, where T_{Debye} is the Debye temperature.

Groeneveld *et al.*[1,2] have measured the relaxation time τ in Au and Ag as a function of temperature ($T=10$–300 K) and laser-energy density ($U_{laser}=0.3$–$1.3\ \mathrm{J\,cm^{-3}}$) using the femtosecond pump-probe technique. Their experimental data were inconsistent with the TTM predictions for τ versus T and τ versus U_{laser}, which led Groeneveld *et al.* to consider the nonthermal electron model. Using a simple estimate, they pointed out that the relaxation time within the electron system is comparable to the electron-phonon relaxation time. Instead of assuming a thermal equilibrium distribution for the electrons, they numerically solved the Boltzmann equation for *electrons* with electron-electron and electron-phonon scattering, starting from an initial nonthermal electron distribution created by a laser pulse. (Based on the fact that the phonon specific heat is much larger than the electron specific heat, phonons were assumed to have a thermal distribution with a time independent T.) This simulation could explain experimental data down to about 50 K. Although the work of Groeneveld *et al.* proposed the essential idea of a *nonthermal electron system*, their analysis focused on temperatures above 50 K, and excluded the low-T region where the most striking difference between the TTM ($\tau \sim T^{-3}$) and the experimental data (almost T independent τ) occurs. Therefore, we undertake a more detailed analysis, particularly focused on the low-T region, to understand the difference in relaxation dynamics between thermal and nonthermal electrons in normal metals as well as in heavy-fermion metals.

B. Relaxation dynamics between nonthermal electrons and phonons

We consider the coupled Boltzmann equations for both *electrons and phonons*, with electron-electron and electron-phonon scattering included.[14] The Boltzmann equations with momentum indices are transformed into the following equations with energy indices for a model with isotropic Debye phonons and electrons with an isotropic parabolic dispersion relation. In terms of electron and phonon distributions at time t, $f_\epsilon(t)$ and $b_\omega(t)$, and the electron and phonon DOS, $D_e(\epsilon)$ and $D_p(\omega)$, where ϵ and ω represent the electron and phonon energies, the coupled Boltzmann equations are[15–17]

$$\frac{df_\epsilon}{dt}=\left[\frac{df_\epsilon}{dt}\right]_{ep}+\left[\frac{df_\epsilon}{dt}\right]_{ee}, \tag{2}$$

$$\frac{db_\omega}{dt}=\left[\frac{db_\omega}{dt}\right]_{ep}, \tag{3}$$

with the collision integrals

$$\begin{aligned}\left[\frac{df_\epsilon}{dt}\right]_{ep}=\int d\omega\, K_{ep}\{[&f_{\epsilon+\omega}(1-f_\epsilon)(b_\omega+1)\\ &-f_\epsilon(1-f_{\epsilon+\omega})b_\omega]D_p(\omega)D_e(\epsilon+\omega)\\ &+[f_{\epsilon-\omega}(1-f_\epsilon)b_\omega-f_\epsilon(1-f_{\epsilon-\omega})(b_\omega+1)]\\ &\times D_p(\omega)D_e(\epsilon-\omega)\},\end{aligned} \tag{4}$$

$$\begin{aligned}\left[\frac{db_\omega}{dt}\right]_{ep}=\int d\epsilon K_{ep}[&-b_\omega f_\epsilon(1-f_{\epsilon+\omega})\\ &+(b_\omega+1)f_{\epsilon+\omega}(1-f_\epsilon)]D_e(\epsilon)D_e(\epsilon+\omega),\end{aligned} \tag{5}$$

$$\begin{aligned}\left[\frac{df_\epsilon}{dt}\right]_{ee}=\int d\epsilon' d\epsilon'' \tfrac{1}{2}K_{ee}[&-f_\epsilon f_{\epsilon'}(1-f_{\epsilon''})(1-f_{\epsilon+\epsilon'-\epsilon''})\\ &+(1-f_\epsilon)(1-f_{\epsilon'})f_{\epsilon''}f_{\epsilon+\epsilon'-\epsilon''}]\\ &\times D_e(\epsilon')D_e(\epsilon'')D_e(\epsilon+\epsilon'-\epsilon'').\end{aligned} \tag{6}$$

The linear dependence of the electron-phonon scattering rate on the acoustic-phonon energy ω [see, e.g., Eq. (26.42) in Ref. 15] has been canceled out by a $1/\omega$ factor which originates from changing momentum indices to energy-indices, so that K_{ep} is an energy-independent constant. K_{ep} and K_{ee} include the squares of the scattering matrix elements and all other numerical factors, and have the units of energy/time.

In the remainder of this section, we consider only light electron systems (normal metals). The above Boltzmann equations, with electron and phonon DOS explicitly included, show why the electron-electron relaxation time is comparable to the electron-phonon relaxation time at low temperatures. The relaxation rate depends on the square of the scattering matrix elements (i.e., K_{ep} and K_{ee}) and the number of available final states (i.e., D_e and D_p). If we compare Eqs. (4) and (6), even though K_{ee} is typically much larger than K_{ep}, the large disparity between the magnitude of the phonon (D_p) and electron (D_e) DOS expedites the relaxation of electrons with phonons, and hinders electrons from reaching thermal equilibrium. The electron-electron and electron-phonon relaxation times τ_{ee} and τ_{ep} vary with T. In Ref. 2, Groeneveld *et al.* found $\tau_{ee}\sim T^{-2}$ [Eq. (16) of Ref. 2] from Fermi-liquid theory. Figure 1 schematically compares the temperature dependence of τ_{ee} (thick line) and τ_{ep} (thin line), the latter of which is from the TTM results.[2,12] The plot shows that it is likely that at high temperatures the electron system thermalizes within itself faster than the thermalization time with the lattice, whereas at low temperatures electron-electron thermalization becomes slower than the electron-phonon relaxation. More detailed discussion on T-dependent thermal versus nonthermal electron distributions will be given later in this section.

We now discuss the methods and parameter values we used to analyze the above Boltzmann equations. The coupled Boltzmann equations are solved in two different ways. In the first method, an initial condition at $t=0$ is set as a nonthermal electron distribution excited by the laser pulse, $f_\epsilon(t=0)=f_{FD}(\epsilon,T_i)+\Delta f_\epsilon$, and a thermal phonon distribution, $b_\omega(t=0)=b_{BE}(\omega,T_i)$, where T_i, $f_{FD}(\epsilon,T_i)$, and

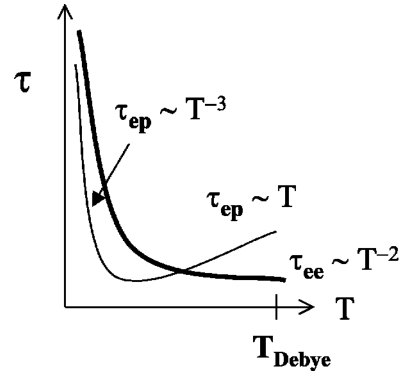

FIG. 1. Schematic plot for the temperature dependence of electron-electron and electron-phonon relaxation times τ_{ee} (thick line) and τ_{ep} (thin line). τ_{ee} is from Eq. (16) in Ref. 2. τ_{ep} is from the TTM calculation, which assumes a *thermal* electron distribution. The ratio between τ_{ee} and τ_{ep} at high T (e.g., T_{Debye} or 300 K) depends on the K_{ee}/K_{ep} ratio. For $K_{ee}/K_{ep}=700$ used in our calculation, $\tau_{ee}<\tau_{ep}$ at $T=T_{Debye}$, as shown in the plot.

$b_{BE}(\omega,T_i)$ represent the initial temperature, Fermi-Dirac, and Bose-Einstein distribution functions before the photoexcitation. We find $f_\epsilon(t)$ and $b_\omega(t)$ at subsequent times by solving the differential equations until both $f_\epsilon(t)$ and $b_\omega(t)$ approach the final thermal distributions at equal T's. A small Δf_ϵ has been chosen so that the final T (T_f) is less than 3 K higher than T_i (even at the lowest T), which simulates the low laser intensity used in the experiments.[7] In the simulation the total electron energy $E_e(t)$ is calculated at each time step, and the instantaneous relaxation time $\tau(t)$ is evaluated using $E_e(t)$ at three consecutive time steps.[18]

In the second method, we perform a linear stability analysis around the final states $f_{FD}(\epsilon,T_f)$ and $b_{BE}(\omega,T_f)$ by expanding the coupled Boltzmann equations, Eqs. (2) and (3), linearly in $\delta f_\epsilon(t)$ and $\delta b_\omega(t)$, where $f_\epsilon(t)=f_{FD}(\epsilon,T_f)+\delta f_\epsilon(t)$ and $b_\omega(t)=b_{BE}(\omega,T_f)+\delta b_\omega(t)$. The zeroth-order terms of the expansion vanish on both sides of the equations, because they correspond to the final equilibrium state. With $\delta f_\epsilon(t)=v_\epsilon^e e^{-t/\tau}$, $\delta b_\omega(t)=v_\omega^p e^{-t/\tau}$, and discretized N electron and M phonon energy levels, the linear differential equations can be cast into an eigenvalue problem of an $(N+M)\times(N+M)$ matrix, the solution of which gives $-1/\tau$ (eigenvalues) and the normal modes of the relaxation. Two of the normal modes have an unphysical infinite relaxation time τ, which originates from total energy and total electron number conservation. The rest of the modes represent all possible relaxation modes of the system. In general, the relaxation of the system can be represented as a linear combination of these modes. By examining the eigenvector of each mode, we find whether the mode predominantly contributes to e-e, p-p, or e-p relaxation. Since the energy-transfer rate from the electron system to the phonon system at time t of a specific mode with relaxation time τ is given by $dE_{e,\tau}(t)/dt=[\int(\epsilon-E_F)(-1/\tau)v_\epsilon^e D_e(\epsilon)d\epsilon]e^{-t/\tau}$, a useful quantity to identify the e-p relaxation modes is the following e-p energy-transfer strength $r_E(i)$:

$$r_E(i)=\frac{1}{\tau(i)}\sum_{n=1}^{N}(\epsilon_n-E_F)v_n^e(i)D_e(\epsilon_n)\Delta\epsilon, \qquad (7)$$

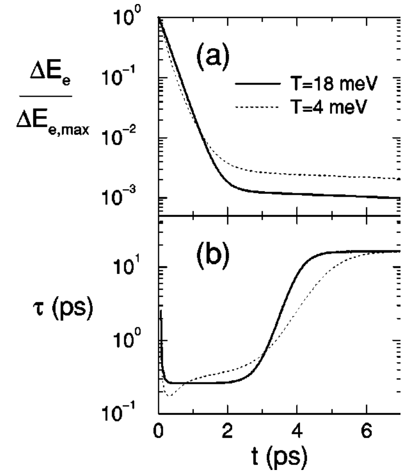

FIG. 2. A typical result of (a) normalized excess electron energy versus time and (b) the instantaneous relaxation time versus time at high T (solid lines, $T=18$ meV$=208$ K) and low T (dotted lines, $T=4$ meV$=46$ K).

where $\Delta\epsilon$ is the energy step size, and $(v_1^e,v_2^e,\ldots,v_N^e,v_1^p,\ldots,v_M^p)_i$ is the normalized eigenvector for mode i with proper overall sign. $r_E(i)$ characterizes the effectiveness of mode i for electron-phonon energy relaxation. The modes which have large r_E dominate in e-p relaxation, and their eigenvectors describe how the relaxation between the electron and phonon systems occurs. The modes with small $r_E(i)$ are either p-p or e-e relaxation modes, and describe how the relaxation within each system happens.

The electron and phonon energy levels are discretized with a step size of 2 meV, which we find small enough that any smaller step size would not change our results even at 10 K (the lowest T of the calculations and experiments). The energy window for the electrons has been chosen to be between -0.15 eV and 0.15 eV with $E_F=0$, which is wide enough in comparison to the highest T of the calculations ($\sim$300 K). Since the typical bandwidth of normal metals is of the order of eV, the electron DOS for normal metals is assumed to be constant within this energy window. Fitting the experimental electronic specific-heat (C_e) data, we obtain $D_e=2.1$ eV^{-1} f.u.$^{-1}$ spin^{-1} for $LuAgCu_4$,[9] which has been used for all of the results presented in this section. Phonons are modeled by the Debye phonon model. Since only longitudinal phonon modes couple with electrons in the isotropic electron and phonon model,[17] we use the longitudinal phonon DOS with a Debye energy $\omega_D=24$ meV (Ref. 10) and six atoms per formula unit, $D_p(\omega)=18\omega^2/\omega_D^3$ per formula unit, in the Boltzmann equations. For most of the calculations, we use $K_{ee}/K_{ep}=700$ (see Figs. 3, 5, and related discussion for this choice of K_{ee}/K_{ep} ratio), and K_{ep} has been chosen as $K_{ep}=0.93$ eV/ps for normal metals by fitting experimental data with the results of the calculation (see Fig. 3).

We now discuss the results obtained from the first method. Figure 2 shows a typical result of normalized excess electron energy, $\Delta E_e/\Delta E_{e,max}$ versus time (t), and τ (instantaneous relaxation time) versus t at high (solid lines) and low (dotted lines) temperatures, where $\Delta E_e(t)=E_e(t)$

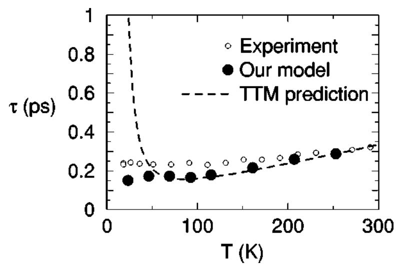

FIG. 3. Relaxation time τ calculated from the coupled Boltzmann equations for $LuAgCu_4$, along with experimental data and the TTM prediction (Ref. 7).

$-E_e(t=\infty)$ and $\Delta E_{e,max}=\Delta E_e(t=0)$. Two different stages of relaxation can be identified for high-T results. During the intermediate time between 0.3 ps and 2 ps (as mentioned earlier, the time scale in picoseconds is obtained by using $K_{ee}/K_{ep}=700$ and $K_{ep}=0.93$ eV/ps), the energy transfer from electrons to phonons is fast. After more than 99% of the excess electron energy is transferred to phonons, a slow relaxation (about 100 times slower than the intermediate stage) appears. The changes of distribution functions at different time stages show that the fast relaxation during the intermediate time corresponds to electron-phonon relaxation, whereas the later slow relaxation corresponds to phonon-phonon thermalization processes.[19] The relaxation behavior is independent of the initial conditions, i.e., the form of Δf_ϵ, except at *very* early stages of the relaxation, namely, $t<0.3$ ps in Fig. 2. Since the changes in electron distribution during the late stage are expected to be unobservable due to experimental noise, we identify the intermediate stage τ [$t=0.3\sim2$ ps for the solid line in Fig. 2(b)] as the one measured experimentally at high T. As T is lowered in the simulation, the well-defined flat intermediate time region in the τ versus t plot is replaced by a gradually changing τ with a minimum as shown in Fig. 2(b). This indicates multiple relaxation times, a sign of a nonthermal electron distribution. As done in the experiments, we find the best-fitting single relaxation time through a linear fit of $\ln|dE_e/dt|$ versus t, which is close to the minimum τ of the dotted line in Fig. 2(b).

The τ's obtained at various T's are plotted in Fig. 3 (solid circles) along with the experimental data (open circles) for $LuAgCu_4$ and the TTM prediction (dashed line, see Ref. 7). The time unit has been scaled to fit the experimental data at high T, which gives $K_{ep}=0.93$ eV/ps as mentioned previously. The fit does not uniquely determine K_{ee}, as long as K_{ee} is smaller than or similar to $700K_{ep}$. The results show reasonable agreement with experimental data, including the region below 50 K, where the TTM predicts strikingly different $\tau\sim T^{-3}$ behavior (Refs. 2 and 12). By comparing df/dt and $-df_{FD}/dT$, we examine whether the electron system approaches the final equilibrium state while maintaining a thermal distribution or not, as shown in Fig. 4 at high and low T's. At high T [Fig. 4(a)], the two curves coincide with each other [indistinguishable in Fig. 4(a)], implying that the electron system has a thermal distribution. However, at low T [Fig. 4(b)], df/dt (solid line with solid circles) has a width of the order of the Debye temperature (T_{Debye}) instead

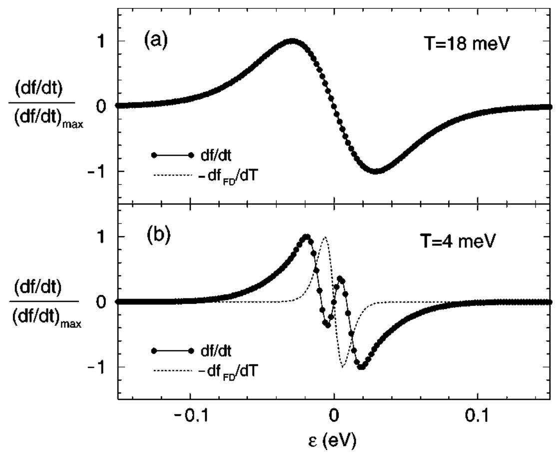

FIG. 4. Normalized df/dt compared with normalized $-df_{FD}/dT$ at (a) high T and (b) low T. For high T, the two lines coincide.

of T, which is the width of $-df_{FD}/dT$ (dotted line).[20] The results clearly show that at low temperatures the electron system does not have a thermal distribution, which agrees with the previous discussion in relation to Fig. 1.

The effect of a nonthermal electron distribution on the relaxation dynamics becomes even more evident, if we increase K_{ee} to $7000K_{ep}$ so that the electron-electron relaxation is faster than the electron-phonon relaxation even in the low-T region. The result (solid circles) is shown in Fig. 5 along with TTM prediction (line). In this case, the electron system has a thermal distribution in the whole T range, and the TTM prediction $\tau\sim T^{-3}$ is recovered at low T. It is remarkable that our simulation with a large K_{ee} recovers the TTM prediction in spite of the fact that our Boltzmann equations do not include direct phonon-phonon scattering and, therefore, the phonon distribution is nonthermal except at $t=\infty$. We speculate that the very weak dependence of e-p thermalization dynamics on the phonon distribution (in con-

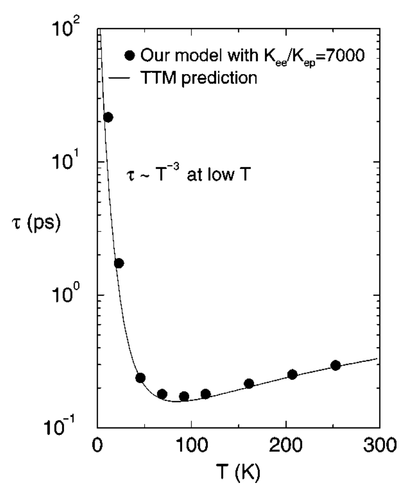

FIG. 5. Solid circles: calculated relaxation time τ from our model for $LuAgCu_4$ for a very large $K_{ee}\geqslant 7000\times K_{ep}$. Line: TTM prediction from Fig. 3. With fast electron-electron relaxation our simulations based on coupled Boltzmann equations recover the TTM prediction $\tau\sim T^{-3}$ at low T.

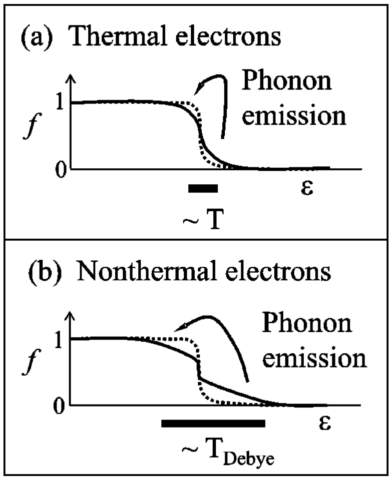

FIG. 6. Schematic pictures explaining different relaxation dynamics for (a) thermal and (b) nonthermal electron distributions at low temperatures. Dotted lines represent the final thermal electron distribution.

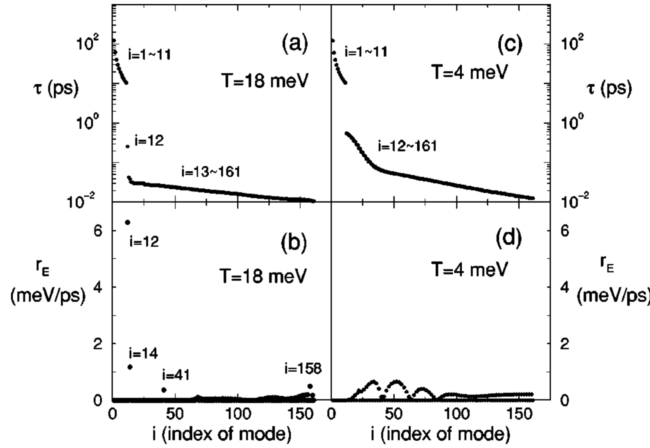

FIG. 7. [(a), (c)] Relaxation time τ and [(b), (d)] e-p energy-transfer strength r_E at [(a), (b)] high T and [(c), (d)] low T calculated by the second method, which linearizes the coupled Boltzmann equations. The index i is assigned in descending order of τ.

trast to the very strong dependence on electron distribution) originates from the characteristics of Bose (versus Fermi) statistics.[21]

We provide a qualitative reason why the thermal electron distribution gives rise to a slow $\tau \sim T^{-3}$ relaxation behavior and the nonthermal electron distribution gives faster and less T-dependent relaxation behavior at low T. As depicted in Fig. 6(a), if the electrons have a thermal distribution at T (solid line), which is slightly higher than the final T (dotted line), the electron-phonon scattering important for the relaxation happens within the energy range of the order of T from E_F. Therefore, the relaxation rate depends on how many phonon modes exist at $\omega < T$. In the Debye phonon model, since $D_p(\omega) \sim \omega^2$, the relaxation rate τ^{-1} is proportional to T^3. In contrast, if the electron distribution is nonthermal [solid line in Fig. 6(b)], then electron-phonon relaxation occurs over an energy range of the order of Debye energy [see also Fig. 4(b)]. This makes the electron-phonon relaxation faster and less T dependent, as indeed observed (Fig. 3).

In the second method, we linearize the coupled Boltzmann equations and calculate eigenvalues and eigenvectors of the matrix. This second method supports and clarifies the results obtained earlier by the first method. With the same discretized energy levels as in the first method, a total of 163 energy levels (151 electron and 12 phonon energy levels) exist in our model, which means a matrix of size 163×163 has to be numerically diagonalized. Two of the 163 eigenmodes are unphysical as discussed earlier. The remaining 161 physical modes have negative eigenvalues, $-1/\tau$, as expected for a stable fixed point, and represent all possible relaxation modes of the system. The τ's at high and low T's are plotted in Figs. 7(a) and 7(c), respectively. The indices of modes i are assigned in descending order of τ. The e-p energy-transfer strength r_E calculated by Eq. (7) for high and low T's is plotted in Figs. 7(b) and 7(d), showing the efficiency of each mode for electron-phonon energy relaxation. At both T's, there exist 11 modes (one less than the number of phonon energy levels) which have a much larger τ than the rest of the modes. For example, at high T these modes are two orders of magnitude slower than the rest of the modes. These slow modes, whose eigenvectors have mostly phonon components and very little electron components, correspond to the late time phonon-phonon relaxation (see Fig. 2). For the high-T results in Figs. 7(a) and 7(b), a single mode with $i=12$ has a large r_E and is very effective in transferring energy from the electron system to the phonon system in comparison to the other modes. This mode has a value of τ identical to the intermediate time τ in Fig. 2 found by the first method, and is well separated from other τ values as seen in Fig. 7(a).[22] The electron part of its eigenvector matches $-df_{FD}/dT$, confirming the results obtained by the first method at high T [Fig. 4(a)], that is, the presence of a thermal electron distribution. Modes with $i=14$, 41, and 158 have smaller r_E values than the $i=12$ mode. Their eigenvectors show that they participate in e-p relaxation, but the electronic parts of the eigenvectors do not match $-df_{FD}/dT$. Their nonthermal behavior seems suppressed in the experiments and in the simulation due to the thermal $i=12$ mode, which has more than five times larger energy-transfer strength r_E. The remainder of modes between $i=13$ and 161 with very small r_E values are mainly e-e thermalization modes. These features change as T is lowered, as shown in Figs. 7(c) and 7(d). Many modes (modes with roughly $r_E > 0.1$ meV/ps) transfer energy from the electrons to the phonons. However, none of their corresponding electronic eigenvectors can be described by $-df_{FD}/dT$, indicating the absence of a well-defined electron temperature during relaxation. This again supports the results of the first method, presented in Fig. 4(b). The rest of the modes between $i=13$ and 161 with r_E very close to zero again correspond to e-e relaxation modes. Importantly, these have larger τ values compared to the high-T case, showing the slowing down of e-e relaxation at low T, consistent with Fig. 1.

Both methods show the importance of a nonthermal electron distribution for the electron-phonon relaxation dynamics at low T for normal metals. In the following section, we

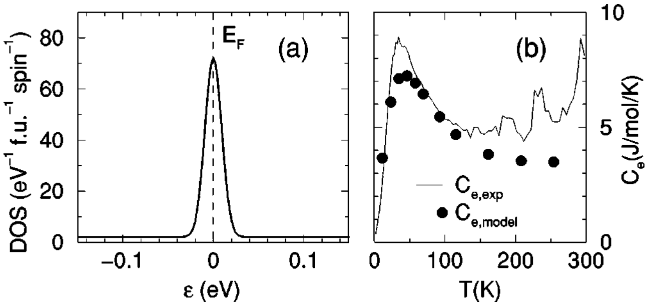

FIG. 8. (a) Model DOS and (b) calculated electron specific heat (solid circles) along with experimental data of C_e (line) for $YbAgCu_4$.

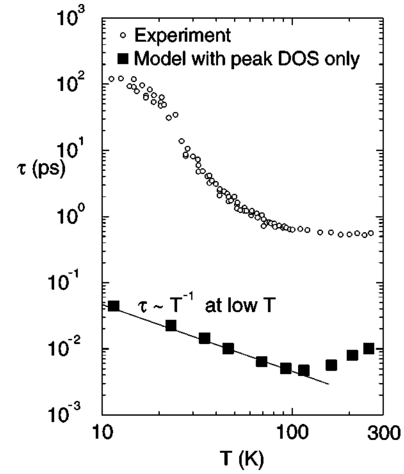

FIG. 9. Relaxation time calculated with the peak DOS only [Eq. (8) and Fig. 8(a)], along with experimental data for $YbAgCu_4$.

discuss how the relaxation dynamics of heavy-fermion compounds are dramatically different from that of normal metals.

III. HEAVY-FERMION MATERIALS

As mentioned in Sec. I, heavy-fermion materials are characterized by a large DOS peak with a width of order T_K near E_F. $YbAgCu_4$ has $T_K \sim 100$ K and is a paramagnetic metal down to the lowest T studied.[10] The interaction between localized f electrons and delocalized conduction electrons in heavy fermion materials is a focus of intensive research in strongly correlated electron systems and has not yet been fully understood. In this paper, we consider the simplest model that captures the basic physics of heavy-fermions, that is, a peak in the DOS near E_F. Even though some theories[23] predict a disappearance of the peak DOS above T_K, we find that the calculated specific heat [Fig. 8(b)] and relaxation time (Fig. 11) have only a weak dependence on the presence or absence of the peak DOS above T_K. (Therefore, neither the relaxation-time data nor the specific-heat data can distinguish whether the peak DOS is present or not above T_K.) In the hybridization gap model,[24] local f levels hybridize with the conduction band and open a gap with DOS peaks above and below the gap. If E_F is located within the peak, not in the gap, the results we will show below have little dependence on whether we use a hybridization gap model or a single-peak DOS model. Therefore, in our simple model, we assume a T-independent single-peak electron DOS as shown in Fig. 8(a). We further simplify the problem by choosing the E_F at the center of the peak, so that the chemical potential is T independent. The peak DOS is described by a Gaussian function with a constant background DOS:

$$D_e(\epsilon) = D_{peak}\exp[-(\epsilon/\Delta)^2] + D_0. \tag{8}$$

The discretized energy step size and energy window are identical to the normal-metal case in Sec. II. We determine the DOS parameters by fitting the electronic specific-heat data, C_e, as shown in Fig. 8(b), and obtain $D_{peak} = 70$ eV^{-1} f.u.$^{-1}$ spin^{-1}, $D_0 = 2.1$ eV^{-1} f.u.$^{-1}$ spin^{-1}, and $\Delta = 13$ meV. D_{peak} is directly related to the linear slope of C_e near $T=0$. Δ is of the order of T_K and determines the temperature of the peak in C_e. D_0 is identical to the electron DOS at E_F for $LuAgCu_4$, and is related to C_e above T_K.

Since $LuAgCu_4$ and $YbAgCu_4$ are isostructural with almost identical atomic masses, we use identical phonon DOS for $LuAgCu_4$ and $YbAgCu_4$.

To gain insight into the nature of the scattering between heavy electrons and phonons, we consider a case in which only heavy electrons with an isotropic parabolic dispersion exist. As in the normal-metal case, we transform the coupled Boltzmann equations with momentum indices into the equations with energy indices. The result is similar to the normal-metal case, Eqs. (4)–(6), except for one important difference: If the Fermi velocity v_F is slower than the sound velocity v_s, where $v_F = (\partial\epsilon/\partial k)_{\epsilon=E_F}$ and $v_s = (\partial\omega/\partial k)_{k\to 0}$, then the phonon integration in the electron-phonon scattering has a lower bound, which represents the blocking of electron-phonon scattering for low-energy phonons and has a great influence on electron-phonon relaxation at low T. Therefore, if $v_F > v_s$, Eqs. (4)–(6) with a peak DOS for D_e can be used to approximately model the relaxation dynamics for both light and heavy electrons, whereas if $v_F < v_s$, appropriate blocking of scattering processes should be imposed upon these equations.

We first consider the case $v_F > v_s$, for which the important physics is simply the increased DOS near E_F given by Eq. (8). We use the same value of K_{ep} and K_{ee} as the $LuAgCu_4$ case in Sec. II. The calculated τ (solid squares) and the experimental data (open circles) shown in Fig. 9 disagree in two respects. First, the calculated τ at around $T = 300$ K is about 60 times less than the observed τ. (Note that, experimentally, both $YbAgCu_4$ and $LuAgCu_4$ have similar τ at ~ 300 K.) This difference is due to the increased electron DOS in the calculation, which enhances the e-p relaxation. An ≈ 60 times smaller K_{ep} would shift the calculated τ in the whole T range by 60 times, but it is unlikely that K_{ep} in $YbAgCu_4$ would be smaller than K_{ep} in $LuAgCu_4$ in such a drastic way. Second, and more importantly, the divergence of calculated τ's at low T is much weaker than the experimental data. This slow divergence in calculated τ can be understood in the following way. The large electron DOS increases both the electron-electron and

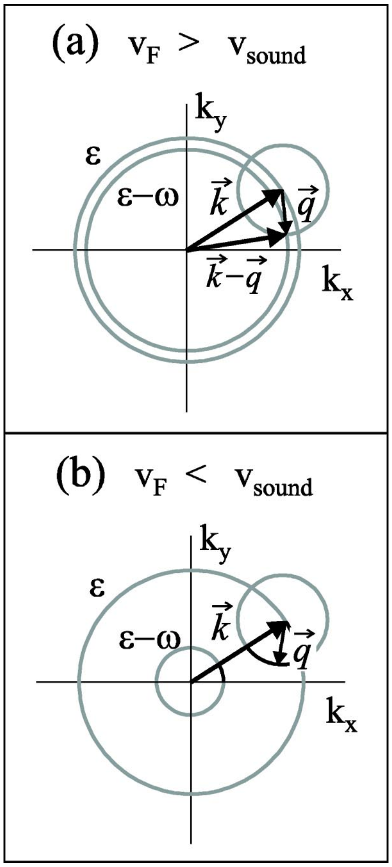

FIG. 10. Schematic pictures explaining different electron-phonon scattering processes for (a) $v_F > v_s$ and (b) $v_F < v_s$ cases. If $v_F < v_s$, then the electron dispersion changes more slowly than the phonon dispersion. Therefore, the distance between the two k-space spheres with energies ϵ and $\epsilon-\omega$ is larger than the phonon momentum q, and no momentum- and energy-conserving scattering process is possible, as shown in (b) in this figure.

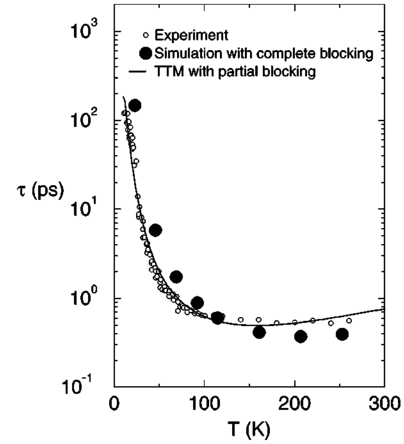

FIG. 11. Solid circles: relaxation time calculated with peaked DOS and blocking of e-p scattering within the peak DOS due to $v_F < v_s$. Open circles: experimental data for $YbAgCu_4$. Solid line: results obtained in Ref. 7 using TTM with partial blocking of the e-p scattering within the peak.

the electron-phonon scattering rates due to the increased number of available final states [see Eqs. (4)–(6)]. However, electron-phonon scattering in Eq. (4) has only one factor of D_e, whereas electron-electron scattering in Eq. (6) has three factors of D_e. Therefore, the electron-electron scattering rate increases much faster than the electron-phonon scattering rate, which makes the electron system thermal and the TTM description valid.[25] According to the calculation of Kaganov *et al.*,[12] $g(T)$ in Eq. (1) goes as $g(T) \sim T^4$ at low T and $g(T) \sim$ const at high T. For normal metals, since $C_e \ll C_p$ even down to 10 K, the TTM relation, Eq. (1), gives $\tau \sim T^{-3}$. In the case of heavy-fermion compounds, C_e is comparable to or larger than C_p at low T, and therefore $C_p \sim T^3$ for the Debye phonons produces $\tau^{-1} \sim T$ as the leading T dependence. Indeed, the low-T divergence of the calculated τ in Fig. 9 can be well described as T^{-1}. Therefore, the discrepancy with experimental data cannot be fixed by simply changing parameters, and it indicates that there is additional physics involved other than the large DOS at the Fermi level to explain a 100-fold increase of τ below T_K.

If we take the approximation that the difference between E_F and the bottom of the heavy electron band is about T_K, then from the isotropic parabolic heavy electron dispersion model and the carrier density of $n = 0.85$ per formula unit measured by the Hall effect for $YbAgCu_4$,[10] we can estimate $v_F \approx 4$ km/sec. Ultrasonic measurements show that the longitudinal sound velocity along the [111] direction is about 4.4 km/sec.[26] This comparison shows that in fact the two velocities are comparable to each other, supporting the possibility of $v_F < v_s$. We should note that experiments such as de Haas–van Alphen are required for a more reliable estimate of v_F. Therefore, we hypothesize that the Fermi velocity is lower than the sound velocity, and discuss how this affects the electron-phonon relaxation dynamics.

As depicted in Fig. 10, if the Fermi velocity is slower than the sound velocity [Fig. 10(b)], then momentum- and energy-conservation requirements prohibit scattering between heavy-electrons and phonons. In the actual heavy-fermion DOS, heavy electron dispersion exists only within the peak DOS around E_F, and electrons outside the peak have a regular light mass. Therefore, the above blocking mechanism applies only when both the initial and final electron states are within the peak of the DOS. If one or both of the states are outside the peak, regular electron-phonon scattering is expected. These effects can be simply incorporated into the simulation by blocking electron-phonon scattering within the peak DOS. The results of the simulation are shown in Fig. 11 as solid circles, for which the blocked energy range is from -24 meV to 24 meV, $K_{ep} = 0.23$ eV/ps, and $K_{ee} = 700 K_{ep}$. This K_{ep} value is smaller than the value for $LuAgCu_4$ case, by about half in terms of the scattering matrix element. It shows reasonable agreement with experimental data (open circles).

Since the electron system has a thermal distribution, the TTM approach, with a similar blocking of electron-phonon scattering within the peak, can be used to describe the relaxation between the electrons and phonons, which was discussed in Ref. 7. In this TTM approach, we also included the possibility that some electron-phonon scattering within the peak is allowed due to the anisotropy of $v_F(\hat{k})$ and $v_s(\hat{k})$, that is, $v_F > v_s$ along some directions and $v_F < v_s$ along other directions. The results were shown as a solid line in Fig. 3 in Ref. 7 and reproduced in Fig. 11 (solid line), which shows good agreement with experimental data.[27]

The physical idea behind the increase of τ below T_K is simple: As T decreases below T_K, or equivalently the width of the DOS peak, since the electron system has a thermal distribution, the main electron-phonon relaxation processes should occur within the peak [see Fig. 6(a)], where the momentum- and energy-conservation laws block the electron-phonon scattering. Therefore, the electron-phonon relaxation time increases very rapidly as T is lowered below T_K.[28] The results show that complete or substantial blocking of electron-phonon scattering processes within the DOS peak is essential to explain the rapid increase of the electron-phonon relaxation time below T_K in $YbAgCu_4$.

IV. SUMMARY

We provide a theoretical analysis of the ultrafast relaxation dynamics observed by femtosecond time-resolved optical spectroscopy in isostructural $LuAgCu_4$ and $YbAgCu_4$; the former is a normal metal and the latter is a heavy-fermion compound. For normal metals, we find that a nonthermal electron distribution is responsible for a temperature-independent electron-phonon relaxation time at low temperatures, instead of a T^{-3}-divergent behavior predicted by the two-temperature model. For heavy-fermion compounds, we find that prohibiting electron-phonon scattering within the density-of-states peak near the Fermi energy is crucial to explain the rapid increase of the electron-phonon relaxation time below the Kondo temperature. On the basis of the estimated Fermi velocity and the measured sound velocity, we propose the hypothesis that the slower Fermi velocity compared to the sound velocity provides this blocking mechanism due to energy- and momentum-conservation laws. We find good agreement between the experimental data and our model for both normal metals and heavy-fermion compounds.

ACKNOWLEDGMENTS

We thank V. V. Kabanov for useful discussions. This work was supported by U.S. DOE.

*Present address: ''J. Stefan'' Institute, Jamova 39, SI-1000, Ljubljana, Slovenia.

[1] R.H.M. Groeneveld, R. Sprik, and A. Lagendijk, Phys. Rev. B **45**, 5079 (1992).

[2] R.H.M. Groeneveld, R. Sprik, and A. Lagendijk, Phys. Rev. B **51**, 11 433 (1995).

[3] S.D. Brorson, A. Kazeroonian, J.S. Moodera, D.W. Face, T.K. Cheng, E.P. Ippen, M.S. Dresselhaus, and G. Dresselhaus, Phys. Rev. Lett. **64**, 2172 (1990).

[4] C.J. Stevens, D. Smith, C. Chen, J.F. Ryan, B. Podobnik, D. Mihailovic, G.A. Wagner, and J.E. Evetts, Phys. Rev. Lett. **78**, 2212 (1997); J. Demsar, B. Podobnik, V.V. Kabanov, Th. Wolf, and D. Mihailovic, *ibid.* **82**, 4918 (1999).

[5] J. Demsar, K. Biljaković, and D. Mihailovic, Phys. Rev. Lett. **83**, 800 (1999).

[6] R.D. Averitt, A.I. Lobad, C. Kwon, S.A. Trugman, V.K. Thorsmølle, and A.J. Taylor, Phys. Rev. Lett. **87**, 017401 (2001).

[7] J. Demsar, R.D. Averitt, K.H. Ahn, M.J. Graf, S.A. Trugman, V.V. Kabanov, J.L. Sarrao, and A.J. Taylor, Phys. Rev. Lett. **91**, 027401 (2003).

[8] P.G. Pagliuso, C. Rettori, S.B. Oseroff, J. Sarrao, Z. Fisk, A. Cornelius, and M.F. Hundley, Phys. Rev. B **56**, 8933 (1997).

[9] $LuAgCu_4$ has a 15 times larger density of states per formula unit at the Fermi energy (E_F) compared to Ag due to the large number of bands at E_F, not due to the hybridization of local f levels and conduction levels.

[10] J.L. Sarrao, C.D. Immer, Z. Fisk, C.H. Booth, E. Figueroa, J.M. Lawrence, R. Modler, A.L. Cornelius, M.F. Hundley, G.H. Kwei, J.D. Thompson, and F. Bridges, Phys. Rev. B **59**, 6855 (1999); J.M. Lawrence, P.S. Riseborough, C.H. Booth, J.L. Sarrao, J.D. Thompson, and R. Osborn, *ibid.* **63**, 054427 (2001).

[11] The Sommerfeld coefficient γ for $YbAgCu_4$ is 210 mJ/mol K^2, (Ref. 10) which corresponds to a 300 times larger DOS at E_F compared to Ag.

[12] M.I. Kaganov, I.M. Lifshitz, and L.V. Tanatarov, Zh. Éksp. Teor. Fiz. **31**, 232 (1956) [Sov. Phys. JETP **4**, 173 (1957)]; S.I. Anisimov, B.L. Kapeliovitch, and T.L. Perel'man, *ibid.*, **66**, 3776 (1974) [*ibid.* **39**, 375 (1974)]; P.B. Allen, Phys. Rev. Lett. **59**, 1460 (1987).

[13] The TTM result is found from $C_1(dT_1/dt) = -C_2(dT_2/dt) = -g(T)(T_1 - T_2)$.

[14] We have examined the effects of phonon-phonon scattering, and found that it has a negligible effect on the electron-phonon relaxation time.

[15] N.W. Ashcroft and N.D. Mermin, *Solid State Physics* (Holt, Rinehart and Winston, New York, 1976), Chaps. 16 and 26.

[16] L.D. Landau and E.M. Lifshitz, *Physical Kinetics*, Course on Theoretical Physics Vol. 10 (Pergamon, Oxford, 1981).

[17] J.M. Ziman, *Electrons and Phonons* (Oxford University Press, London, 1972).

[18] From the relation $\tau = (-dE_e/dt)/(d^2E_e/dt^2)$ for $E_e(t) = E_0 + \Delta E \exp(-t/\tau)$, we use $\tau(t) = -[E_e(t+dt) - E_e(t-dt)]dt/\{2[E_e(t+dt) - 2E_e(t) + E_e(t-dt)]\}$.

[19] The phonon-phonon thermalization process occurs via electron-phonon scattering, since our Boltzmann equations do not include direct phonon-phonon scattering. For example, a high-energy phonon is absorbed by an electron, which emits two low-energy phonons.

[20] The presence of the extra feature near E_F depends on details of the parameter values and time at which df/dt is evaluated. When this feature is present, as shown in Fig. 4(b), it is partly due to electrons heating up near E_F through electron-electron scattering. [Since electron-electron scattering conserves total electron energy, $(df/dt)_{ee}$ must cross zero at least three times.]

[21] Contrary to the assumption of Groeneveld *et al.* (Refs. 1 and 2), the large phonon specific heat compared to the electron specific heat may not be the reason why TTM results apply to nonthermal phonons, because our simulation agrees with TTM predictions even when the electron specific heat is larger than the

phonon specific heat, as shown in Sec. III (see the discussion of Fig. 9).

[22] When the step size for energy discretization is reduced by half, the gaps in τ between this single mode and the edges of the continuum-like faster and slower τ's do not change. This singular behavior deserves future theoretical studies.

[23] P.G. McQueen, D.W. Hess, and J.W. Serene, Phys. Rev. B **50**, 7304 (1994); B.N. Bickers, D.L. Cox, and J.H. Wilkins, *ibid.* **36**, 2036 (1987); B. Horvatić, D. Šokčević, and V. Zlatić, *ibid.* **36**, 675 (1987).

[24] A.C. Hewson, *The Kondo Problem to Heavy Fermions* (Cambridge University Press, Cambridge, 1993), Chap. 10.

[25] We find that the electron thermalization recovers the TTM predictions, as in normal metals (see Fig. 5).

[26] S. Zherlitsyn, B. Lüthi, B. Wolf, J.L. Sarrao, Z. Fisk, and V. Zlatic, Phys. Rev. B **60**, 3148 (1999).

[27] The hypothesis that the relation $v_F < v_s$ provides the blocking mechanism suggests that the heavy-fermion metals with lighter effective masses may show relaxation dynamics qualitatively different from that of $YbAgCu_4$.

[28] Even when the electron DOS is *T* dependent, as long as the peak width in the DOS does not increase faster than *T*, the results do not change much.